

Global Biogeochemical Cycles

RESEARCH ARTICLE

10.1029/2020GB006578

Key Points:

- In the California Current, submesoscale currents intensify nutrient subduction near the coast and nutrient delivery to the surface offshore
- Submesoscale currents drive a reduction in productivity, new production, and phytoplankton size near the coast and an increase offshore
- Seasonality modulates the biogeochemical effects of submesoscale, with stronger effects inshore during upwelling and offshore in wintertime

Supporting Information:

- Supporting Information S1

Correspondence to:

F. Kessouri and D. Bianchi,
faycalk@sccwrp.org;
dbianchi@atmos.ucla.edu

Citation:

Kessouri, F., Bianchi, D., Renault, L., McWilliams, J. C., Frenzel, H., & Deutsch, C. A. (2020). Submesoscale currents modulate the seasonal cycle of nutrients and productivity in the California Current System. *Global Biogeochemical Cycles*, *34*, e2020GB006578. <https://doi.org/10.1029/2020GB006578>

Received 3 MAR 2020

Accepted 18 SEP 2020

Accepted article online 10 OCT 2020

Submesoscale Currents Modulate the Seasonal Cycle of Nutrients and Productivity in the California Current System

Fayçal Kessouri^{1,2} , Daniele Bianchi² , Lionel Renault^{2,3} , James C. McWilliams² , Hartmut Frenzel⁴ , and Curtis A. Deutsch⁴

¹Department of Biogeochemistry, Southern California Coastal Water Research Project, Costa Mesa, USA, ²Department of Atmospheric and Oceanic Sciences, University of California Los Angeles, Los Angeles, CA, USA, ³Laboratoire d'Etudes en Géophysique et Océanographie Spatiales, University of Toulouse, IRD, CNRS, CNES, UPS, Toulouse, France, ⁴School of Oceanography, University of Washington, Seattle, WA, USA

Abstract In the California Current, subduction by mesoscale eddies removes nutrients from the coastal surface layer, counteracting upwelling and quenching productivity. Submesoscale eddies are also ubiquitous in the California Current, but their biogeochemical role has not been quantified yet in the region. Here, we present results from a physical-biogeochemical model of the California Current run at a resolution of 1 km, sufficient to represent submesoscale dynamics. By comparing it with a coarser simulation run at 4 km resolution, we demonstrate the importance of submesoscale currents for the seasonal cycles of nutrients and organic matter and highlight the existence of different regimes along a cross-shore gradient. In the productive coastal region, submesoscale currents intensify quenching and reduce productivity, further counteracting wind-driven upwelling. In the offshore oligotrophic region, submesoscale currents enhance the upward transport of nutrients, fueling a dramatic increase in new production. These effects are modulated by seasonality, strengthening near the coast during upwelling and offshore in wintertime. The intensification of the transport by submesoscale eddies drives an adjustment of the planktonic ecosystem, with a reduction of plankton biomass, productivity, and size near the coast and an increase offshore. In contrast, organic matter export by sinking particles and subduction of detritus and living cells are enhanced nearly everywhere. Similar processes are likely important in other regions characterized by seasonal upwelling, for example, other eastern boundary upwelling systems.

1. Introduction

The California Current is characterized by seasonally intensified equatorward winds that drive offshore surface flow, upwelling, and alongshore currents (e.g., Marchesiello et al., 2003). Coastal upwelling promotes periodic cold water and nutrient injections to the euphotic zone, which fuel high biological productivity and support important marine resources (e.g., Chavez & Messié, 2009; Cochrane et al., 2009). The surface density gradients generated by upwelling sustain in turn an energetic field of mesoscale eddies and filaments, which extend hundreds of kilometers offshore along the coast (Capet, McWilliams, et al., 2008; Renault et al., 2016).

Advection by mesoscale eddies is the dominant mechanism driving offshore transport of heat, salt, and nutrients (Capet, McWilliams, et al., 2008; Nagai et al., 2015), expanding the area of high productivity beyond shelf waters (Chavez & Messié, 2009). This eddy transport also subducts nutrients and freshly formed organic matter along isopycnals that outcrop near the coast and deepen toward the oligotrophic region offshore (Nagai et al., 2015), reducing the rates of photosynthesis in a process known as “eddy quenching” of productivity (Gruber et al., 2011; Lathuilière et al., 2010; Nagai et al., 2015; Omand et al., 2015; Renault et al., 2016; Stukel et al., 2017). Subduction by mesoscale eddies also supplies organic matter to the aphotic ocean, supporting remineralization of carbon and nutrients thousands of kilometers away from the coastal region (Lovecchio et al., 2018).

Less is known about the biogeochemical role of submesoscale currents in upwelling systems. Submesoscale currents, with horizontal scales of few kilometers or less, are ubiquitous near the surface, fueled by available potential energy and sustained by weak vertical stratification, small-scale turbulence, and straining by the mesoscale circulation (Capet, Campos, et al., 2008; Capet, Klein, et al., 2008; Capet, McWilliams,

et al., 2008; McWilliams, 2016). Ageostrophic circulation associated with submesoscale currents tends to restratify the mixed layer (Boccaletti et al., 2005; McWilliams, 2016) driving vigorous vertical velocities (Lévy et al., 2001; Mahadevan, 2016), with a characteristic enhancement of cyclonic and downwelling motions (McWilliams, 2016; Thomas et al., 2008).

In stratified, oligotrophic regions, submesoscale currents tend to increase productivity by intensifying the delivery of nutrients to the upper layer (Lévy et al., 2001; Mahadevan, 2016). In regions of deep mixed layers, where light rather than nutrients limits phytoplankton growth, restratification of the mixed layer by the submesoscale circulation enhances productivity by stabilizing the water column, extending the growth period of phytoplankton, and initiating blooms (Mahadevan, 2016; Mahadevan et al., 2012). In parallel, submesoscale subduction along fronts enhances export of phytoplankton and organic matter-rich waters from the surface, as observed both in high-latitude regions during phytoplankton blooms (Omand et al., 2015) and in eastern boundary upwelling systems (Stukel et al., 2017).

The picture that emerges is that of significant but regionally and temporally variable effects of submesoscale currents on biogeochemistry (Lévy et al., 2018). In the California Current System, temporal and spatial modulations of submesoscale currents are especially important, because of the strong cross-shore biogeochemical gradients, the energetic mesoscale eddy field, and the large seasonality of these features (Gruber et al., 2011; Nagai et al., 2015). However, a consistent picture of the modulation of nutrient cycles and productivity by submesoscale currents in this region is still missing.

The goal of this study is twofold. First, we aim at drawing a consistent picture of the seasonal cycles of nitrogen in the California Current System, when submesoscale processes are explicitly represented. Second, we investigate the impacts of submesoscale circulation on biogeochemistry, their spatial and temporal modulation, and the consequences for the marine ecosystem in the region. This work is based on a realistic, submesoscale-permitting numerical simulation of the California Current, carried out for a period of 10 years, which we compare to a similar simulation that only resolves mesoscale processes. We focus on the variability of nitrate (NO_3^-) transport, since NO_3^- is the main limiting nutrient in the region, and the resulting impacts on primary production and organic matter transport.

The rest of the paper is organized as follows: Section 2 describes the model formulation and setup, the methods, and a short validation of the model solutions; sections 3 and 4 discuss the surface nitrogen budget of the California Current, with special focus on vertical fluxes and their modulation by submesoscale processes; section 5 investigates the implications for the planktonic ecosystem and organic matter export; and section 6 concludes the paper.

2. Modeling Approach

2.1. Configuration and Experiments

The numerical model configuration used in this study is similar to that employed by Renault, McWilliams, et al. (2020) and Deutsch et al. (2020). We refer the reader to those papers for a detailed description of the model setup and boundary forcings. The oceanic model component consists of the Regional Ocean Modeling System, ROMS (Shchepetkin, 2015; Shchepetkin & McWilliams, 2005), a primitive-equation, hydrostatic, topography-following (i.e., σ coordinate) ocean model. We compare two simulations that only differ in the horizontal grid scale, domain size, and time step (Figure 1). As in Renault, Molemaker, et al. (2016) the coarser domain (Figure 1) spans the entire U.S. West Coast, from Baja California to Vancouver Island. This grid is composed of 437×662 cells, with a nominal resolution of $dx = 4$ km, and the time step is 600 s. The output from the 4 km solution is used to drive a smaller, finer-scale configuration extending from Tijuana to Cape Mendocino (Figure 1). This finer grid is composed of $770 \times 1,440$ cells, with a nominal resolution of $dx = 1$ km, and the time step is 150 s. Both configurations have the same 60 σ coordinate vertical levels using the stretching function described in (Shchepetkin & McWilliams, 2009). Output for both simulations is saved as 1 day averages.

The 4 km simulation is initialized and forced at the open boundaries by a preexisting northeast Pacific ROMS solution at 12 km resolution and is run for the period 1995–2010, after a spin-up of 1 year. The 1 km simulation is initialized and forced from the 4 km model, starting in October 1996 and ending in December 2006. Both configurations are forced at the surface by hourly outputs from an atmospheric simulation with the Weather Research and Forecast model (WRF06) (Skamarock & Klemp, 2008) run at 6 km resolution over a

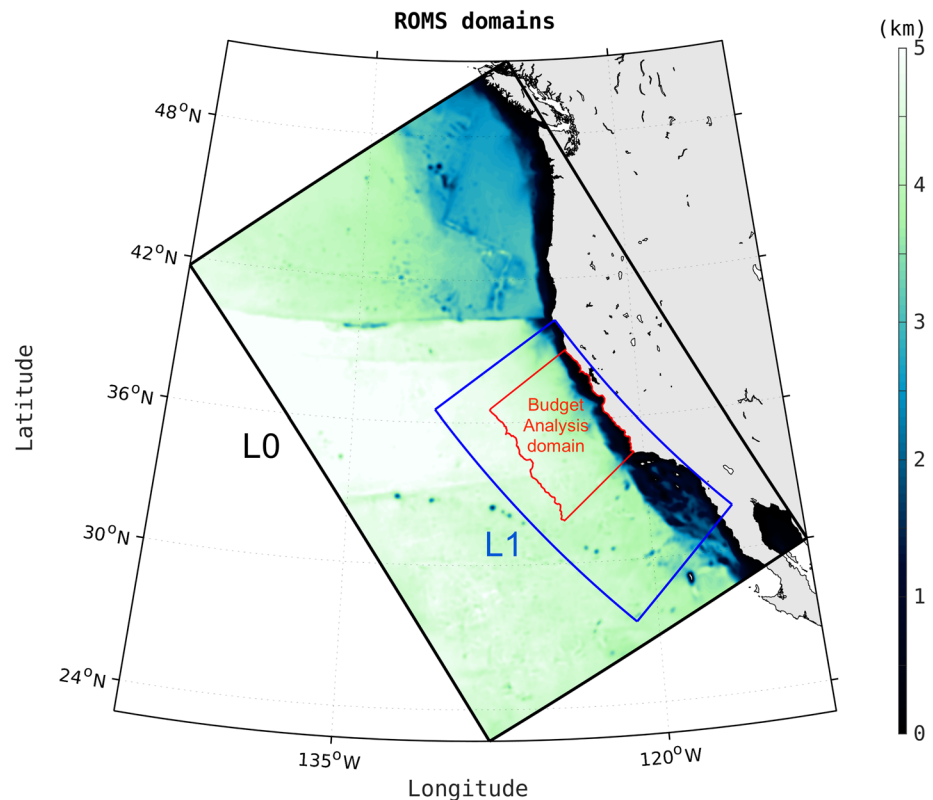


Figure 1. Model domains and analysis region drawn on top the model topography. The outer black box shows the domain of the 4 km model configuration. The inner blue box shows the domain of the 1 km model configuration. The red box along the central coast shows the analysis region used to calculate biogeochemical budgets.

domain similar to the 4 km domain (Renault et al., 2016). Both include a wind-current coupling parameterization necessary to attain more realistic simulations of the oceanic (sub)mesoscale activity and circulation (Renault et al., 2016, 2018, 2020).

The physical ROMS model is coupled online to the Biogeochemical Elemental Cycling (BEC) model (Moore et al., 2004). BEC solves the equations for the evolution of six nutrients (NO_3^- , NH_4^+ , NO_2^- , SiO_2 , PO_4^{3-} , and Fe), three phytoplankton groups (small phytoplankton, akin to picoplankton and nanoplankton, large phytoplankton, akin to diatoms, and diazotrophs), a single zooplankton group, dissolved oxygen, dissolved inorganic carbon, alkalinity, and dissolved organic matter (carbon, nitrogen, phosphorus, and iron). A schematic of the biogeochemical model is shown in supporting information Figure S1. All living biological variables are expressed in units of carbon and are connected to other cycles by fixed stoichiometric ratios. Additional details on the BEC configuration, coupling with ROMS, and validation of the biogeochemical solution in the California Current are presented in Deutsch et al. (2020).

2.2. Model Analysis and Diagnostics

2.2.1. Biogeochemical Budgets

To investigate the pathways of nutrient delivery and transformation in surface waters, we focus our analysis on the budgets of NO_3^- and organic nitrogen. NO_3^- is the main form of biologically available dissolved inorganic nitrogen and dominates inputs to the surface by upwelling and mixing. Because nitrogen is the limiting nutrient in the region, and its cycle is tightly coupled to the cycle of phosphorus, we will often refer to NO_3^- simply as nutrient in this paper. The organic nitrogen component includes dissolved organic nitrogen (DON), sinking particulate organic nitrogen (PON), and suspended particles (i.e., phytoplankton and zooplankton). In BEC, sinking PON is not an explicit prognostic tracer, but at each time step the downward flux of sinking PON is calculated in the water column as a function of production and depth-dependent remineralization (Moore et al., 2004).

Tracer budgets are based on the model conservation equations. For NO_3^- , the budget equation can be written as

$$d\text{NO}_3^-/dt = \text{physical transport} + \text{nitrification} - \text{uptake} - \text{denitrification}. \quad (1)$$

Here “physical transport” consists of the divergence of advective and diffusive fluxes, and “uptake,” “nitrification,” and “denitrification” are the main biological sources and sinks of NO_3^- . A detailed description of each of the terms of Equation 1 can be found in Deutsch et al. (2020) and the references therein. A similar equation can be written for organic nitrogen, including production by photosynthesis, transformation by ecosystem processes, and remineralization to the inorganic nitrogen pool. Biogeochemical rates are calculated at the center of each model grid cell, while physical transport fluxes are calculated at the sides of each cell (supporting information Figure S2) from the same domain. Physical fluxes include advection in the alongshore, cross-shore, and vertical directions, and turbulent vertical diffusion. Biogeochemical rates and physical fluxes are calculated online at each time step, saved at daily resolution, and averaged over monthly periods to construct climatologies. The budget of all tracers is closed to numerical precision and scaled up from individual grid cells to three-dimensional regions by numerical integration.

We focus our analysis on the Central and Northern California region, where the strongest seasonal upwelling and eddy activity are observed (Capet, McWilliams, et al., 2008; Huyer, 1983; Renault et al., 2016) and where the bulk of the California Current is found. We exclude the Southern California Bight, which is characterized by recirculation, oligotrophic conditions, and strong topographically driven eddies, and is thus distinct from the rest of the California Current. We extend our analysis, including the calculation of biogeochemical rates, from the coast to the oligotrophic region 450 km offshore, avoiding the 1 km model domain boundary, and from the surface to 50 m depth, which is close to the average vertical limit of the mixed layer in the region (supporting information Figure S2) and where most of the nutrient uptake takes place. Note that within this depth range, uptake by phytoplankton is the dominant biological term in Equation 1, while nitrification and denitrification are negligible. For more detailed calculations of the cross-shore variability in nutrient budgets and biological activity (section 5) we split the analysis domain into 23 subregions perpendicular to the coast, each 20 km wide in the cross-shore direction, and five latitude degrees wide in the alongshore direction (approximately from 34.5°N to 39°N).

2.2.2. Eddy Decomposition of Biogeochemical Fluxes

We separate the total fluxes of tracers into mean and eddy components following a typical Reynolds decomposition. For example, considering vertical advection, we write

$$\overline{wN} = \overline{w}\overline{N} + \overline{w'N'}. \quad (2)$$

Here, w is the vertical velocity component, and N the concentration of a biogeochemical tracer (e.g., NO_3^-). The overbar denotes the monthly mean climatology based on 10 years of model simulation (January 1997 to December 2007), and the ' denotes the deviation from this mean, which removes seasonal variations. We excluded from the analysis the El Niño year 1998, because it is characterized by particularly strong anomalies in vertical stratification, nutricline depth, and nutrient fluxes that differ markedly from all other years and is thus not representative of typical conditions in the California Current.

The Reynolds decomposition is applied to the physical fluxes of biogeochemical tracers along the vertical, alongshore, and cross-shore directions. Total fluxes, \overline{wN} , are estimated online in the model and saved at daily resolution. The mean component of the fluxes, $\overline{w}\overline{N}$, is calculated from daily mean velocities and tracer concentrations. Eddy fluxes, $\overline{w'N'}$, are calculated by difference, based on Equation 2. We find that vertical turbulent fluxes are dominated by the resolved advection, which corresponds to more than 85% of the vertical transport. In the following, unless otherwise noted, we include parameterized vertical mixing in the total vertical flux for simplicity and calculate vertical transport terms at a depth of 50 m.

2.2.3. Analysis of Submesoscale Processes

We estimate the impact of submesoscale currents by considering the difference in nutrient fluxes and transformation rates between the 1 km submesoscale eddy-permitting simulation and the 4 km mesoscale eddy-resolving simulation. The two simulations only differ in the domain size (Figure 1), the resolution, and the time step. Both are dominated by eddy variability, which is chaotic in nature (McWilliams, 2007), requiring comparison in a statistical sense. While variability in eddy fields is substantial at time scales from

months to years, we find that using 10 years of simulation allows us to extract robust differences in the climatological eddy fluxes between the 1 and 4 km configurations. Differences in the statistics of the two solutions are attributed to the transition from mesoscale-resolving to submesoscale-permitting regimes, which in the California Current System occurs at resolutions of approximately 1 km or less (Capet, Campos, et al., 2008).

We also tested a filtering approach to separate mesoscale and submesoscale contributions to tracer transport. Briefly, this approach is based on a spatial filter with horizontal scales of 12 km applied to the 1 km solution, and interpretation of the small-scale fluctuations as submesoscale (Capet, Campos, et al., 2008). This filtering approach produces comparable results as the direct difference between the 4 and 1 km solution. However, the direct difference is easier to compute, analyze and interpret—for example, unlike the filtering approach, it can be applied near the coastline. Thus, we use it as the basis of the rest of the paper.

While we separate eddy from mean transport terms, we do not attempt to explicitly separate mean and eddy contributions in biogeochemical rates. “Eddy reaction rates” arise from the nonlinear nature of the biogeochemical rate equations (e.g., nutrient uptake by phytoplankton and grazing) and small-scale spatial heterogeneity induced by mesoscale and submesoscale variability (Levy & Martin, 2013). Previous work indicates a small but significant role (between 5% and 30% of total rates) for eddy reaction terms (Levy & Martin, 2013; Martin et al., 2015), with most of the contribution caused by mesoscale (100–30 km) heterogeneity, and weaker contributions (<5%) by scales of 30 km or less (Levy & Martin, 2013). Differences between the 1 and 4 km simulations discussed in this paper (section 5) include both the effects of heterogeneity at scales smaller than 4 km (i.e., eddy transport and eddy reaction terms) and changes in the average distribution of tracers (supporting information Figure S3). We leave an explicit separation of these contributions to a future study.

2.2.4. Model Validation and Emergence of Submesoscale

The 1 and 4 km simulations produce an overall similar picture of the large-scale physical circulation and biogeochemical state of the California Current System (supporting information Figures S4 and S5). Both simulations generate similar patterns in the alongshore mean currents (the broad offshore California Current and the inshore subsurface undercurrent), the cross-shore, surface-confined Ekman transport, and the mean upwelling and its intensification along the continental shelf (supporting information Figure S4). They are also characterized by a similar shoaling of isopycnals toward the coast and broadly comparable distributions of mean temperature, salinity, and nutrients (supporting information Figure S5). A detailed validation of the main patterns, seasonal cycle, decadal trends, and regional variability of the physical and biogeochemical solutions, based on the 4 km simulation, is presented in Renault, McWilliams, et al. (2020) and Deutsch et al. (2020). The 4 and 1 km simulations can therefore be compared to separate the effects of submesoscale from those of mesoscale activity.

Consistent with previous work (e.g., Srinivasan et al., 2017 and Capet, Campos, et al., 2008), the 1 km, submesoscale-permitting solution is characterized by (1) increased spectral power at scales of kilometers to tens of kilometers for horizontal velocities (supporting information Figures S6a and S6b), Eddy Kinetic Energy (EKE), and tracer wavenumber spectra (Capet, Campos, et al., 2008); (2) enhanced variability and intermittency of km-scale motions, with more frequent extremes in vorticity (up to 6 times the local Coriolis frequency), divergence, vertical velocity, and horizontal tracer gradients; and (3) pronounced asymmetries in the distributions of vorticity, divergence (supporting information Figures S6c and S6d), and vertical velocities, with dominance of anticyclonic and downwelling extremes which are substantially weaker at 4 km (supporting information Figures S6e–S6g). These results suggest that submesoscale vertical motions are well developed in the 1 km simulation and that they are an important component of vertical nutrient transport. We focus on this hypothesis in the following sections and test it by analyzing the surface budgets of inorganic and organic nitrogen in the 1 km solution and comparing them to the 4 km simulation.

3. Seasonal Nitrogen Budget and Role of Eddy Fluxes

Two distinct regimes of nutrient supply and uptake by phytoplankton can be identified in the coastal and offshore regions of the California Current. Coastal upwelling generally occurs between spring and summer, followed by an increase in surface nutrients, photosynthesis, and production of organic matter (Figure 2a). Oligotrophic conditions characterize the offshore region throughout most of the year, with a wintertime peak in productivity driven by enhanced mixing (Figure 2b).

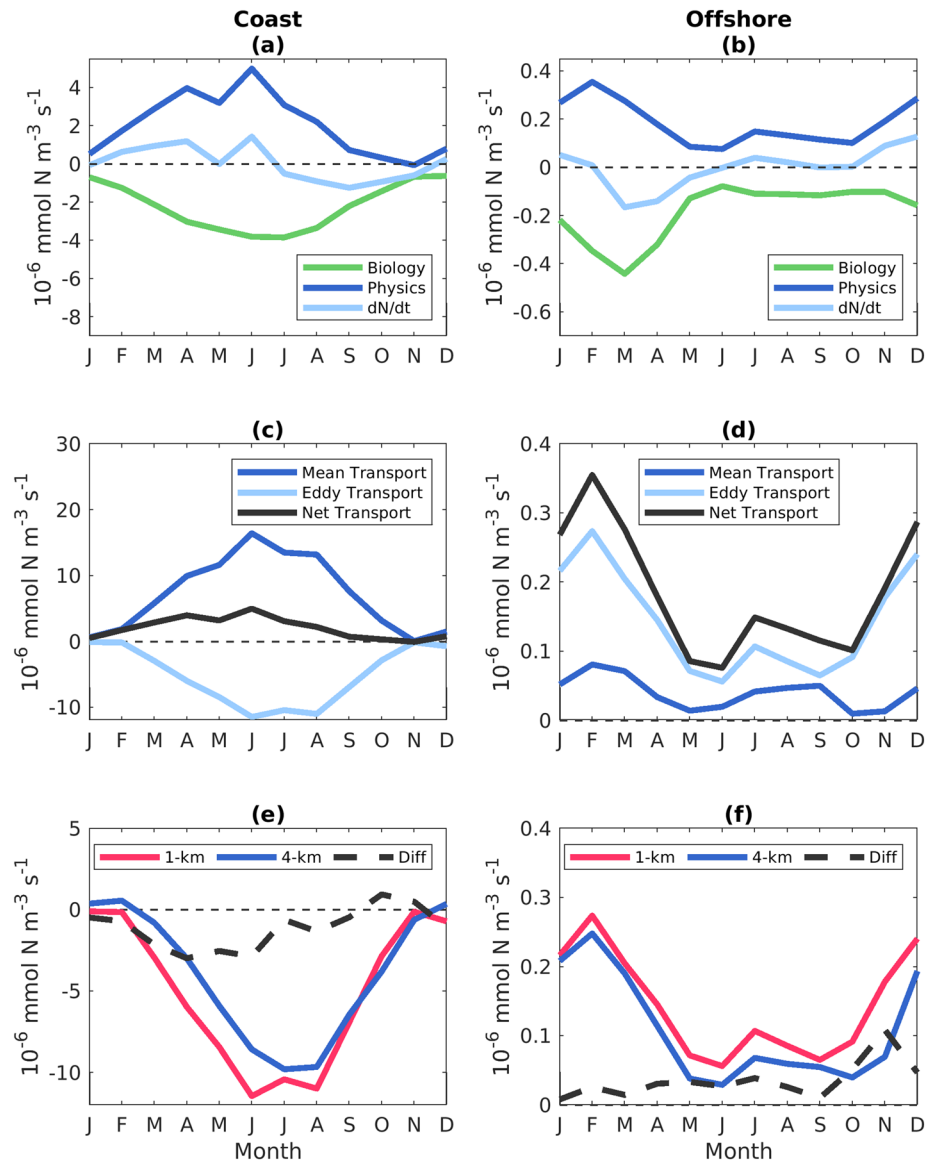


Figure 2. (a, b) The 10 year mean of NO_3^- budget terms ($\text{mmol N m}^{-2} \text{ s}^{-1}$) from the 1 km model simulation in (a) the coastal region (0–40 km) and (b) the offshore region (>250 km) averaged over the upper 50 m depth. Biological terms (dominated by nutrient uptake) are shown in green, physical transport in blue, and the NO_3^- tendency in cyan. (c, d) The 10 year mean of NO_3^- eddy transport (light blue line) ($\text{mmol N m}^{-2} \text{ s}^{-1}$), mean transport (dark blue line), and the net transport (black line) from the 1 km model simulation in (c) the coastal region and (d) the offshore region. (e, f) The 10 year mean of NO_3^- total eddy transport ($\text{mmol N m}^{-2} \text{ s}^{-1}$) in (e) the coastal region and (f) the offshore region. Blue lines show the 4 km solution, red lines the 1 km solution, and black lines the difference between the 1 and 4 km solutions. Positive values show input of nutrients to the surface layer (0–50 m depth), and negative values removal.

In the coastal band (0–40 km), during late winter, spring, and early summer, transport of NO_3^- to the surface (blue line in Figure 2a) is larger than uptake by phytoplankton (green line in Figure 2a) resulting in net nutrient accumulation ($d\text{NO}_3^-/dt > 0$, cyan line in Figure 2a). Increasing nutrients and light throughout the spring and early summer drive an increase in nutrient uptake, with a maximum in July, following the peak in upwelling. From August to the end of the fall, biological consumption outpaces nutrient inputs, leading to a decline in the NO_3^- inventory ($d\text{NO}_3^-/dt < 0$) and productivity.

In the offshore region (>260 km), the largest physical supply and biological uptake of nutrients occur between fall and winter (Figure 2b), when transport is dominated by eddy fluxes (Figure 2d). NO_3^- buildup throughout the fall and early winter fuels an increase in productivity, with a peak by the end of winter.

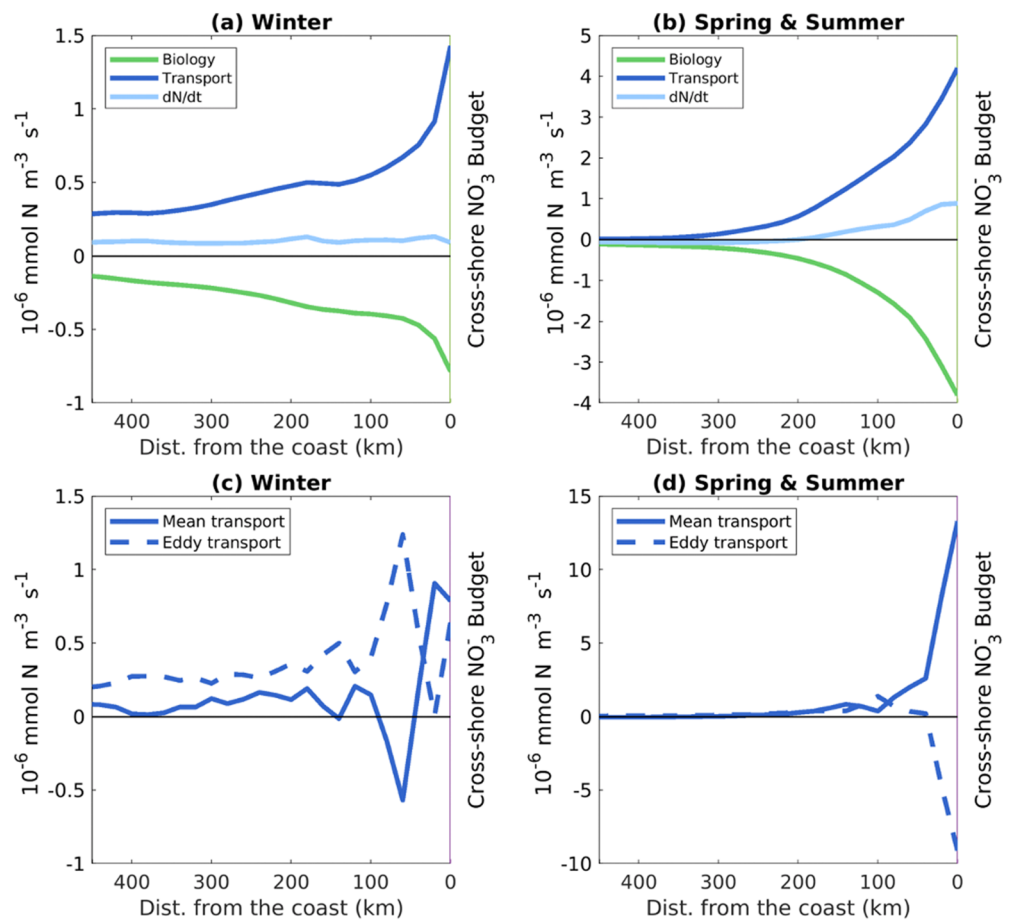


Figure 3. The 10 year mean of NO_3^- budget terms ($\text{mmol N m}^{-2} \text{s}^{-1}$) from the 1 km model solution, as a function of the distance from the coast. (a, b) NO_3^- budget terms, as in Figure 2. (c, d) Transport terms, with mean transport shown by the solid lines, and eddy transport by the dashed lines. All panels show alongshore averages for the analysis region shown in Figure 1, for the winter (a, c) and spring to summer (b, d).

Throughout the spring, nutrient inventories decline, leading to a minimum in primary production by the beginning of summer. Negligible vertical fluxes and a weak lateral transport persist throughout the summer, limiting primary productivity to low background values, generally observed in proximity of deep chlorophyll maxima.

Both vertical and horizontal transport contribute to the supply of NO_3^- to the surface. Vertical fluxes tend to be larger during the periods of highest productivity, both inshore and offshore. In the coastal region, horizontal transport includes nutrients advected meridionally within the California Undercurrent from the southern boundary of the domain. After upwelling, nutrients are also advected offshore by Ekman transport and eddies. This cross-shore flux of nutrients, together with meridional transport along the California Current, supports summertime productivity in the oligotrophic region, at a time when vertical fluxes are severely reduced.

The physical transports hide important eddy and mean contributions, which often counterbalance each other (Figure 2c). At the coast, eddies remove nutrients from the surface, offsetting inputs by the mean transport (Figure 2c). Offshore, eddies supply nutrients to the euphotic zone during the more productive winter season (Figure 2d).

A comparison of the cross-shore distribution of nutrient fluxes, with a separation between eddy and mean components, is shown in Figure 3. In winter, biological NO_3^- uptake is approximately 5 times weaker offshore than at the coast (green line in Figure 3a), but it remains significant in comparison to other seasons (green line in Figure 3b). During upwelling, these cross-shore gradients are intensified.

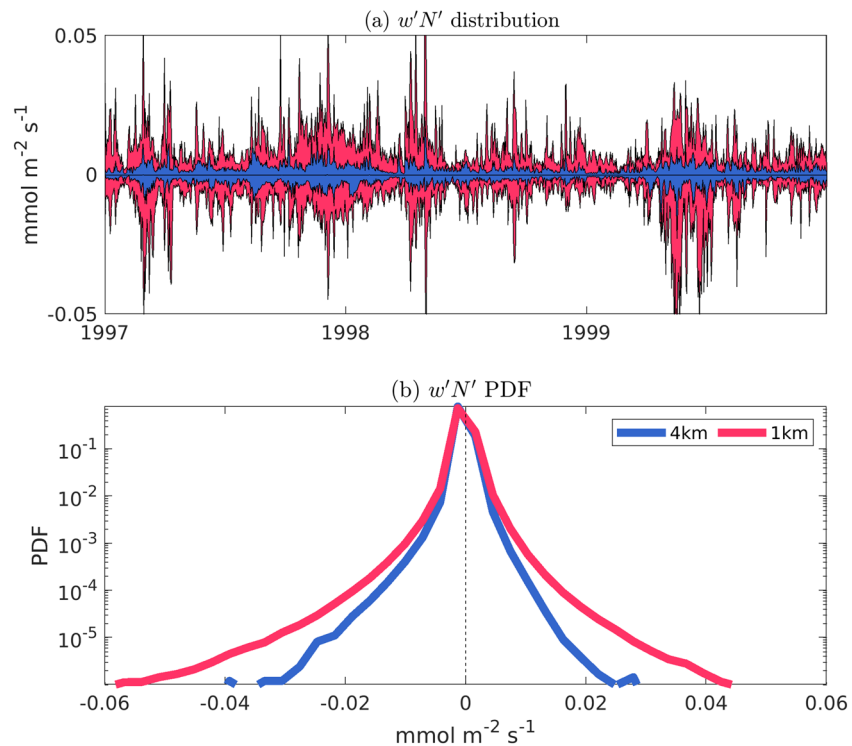


Figure 4. (a) Time series (1997–1999) of the vertical eddy flux of NO_3^- at 50 m depth, for region between the coast and 250 km offshore, calculated based on Equation 2. The minimum and maximum values (i.e., the envelope) of the flux are shown, in blue for the 4 km solution and in red for the 1 km solution. (b) Probability density functions (each normalized to the maximum value) of the vertical eddy flux of NO_3^- at 50 m depth, for the 4 km (dashed line) and 1 km solutions, based on 10 years of simulation.

Depending on the region and time of the year, different processes dominate nutrient supply to the surface. In winter, eddy fluxes dominate nearly everywhere (Figure 3c). Eddy quenching counteracts the mean transport (Figure 3d), subducting nutrients away from the surface. This eddy quenching is generally colocated with the region of strong upwelling and is mainly driven by vertical eddy fluxes.

Further offshore, eddies transition from subducting to supplying nutrients. The location of this transition is seasonally variable: In winter, eddies can only remove nutrients very close (few km) to the coast, and their effect is overall positive throughout the California Current. During upwelling and in summertime, the picture is more complex, with a shift from eddy-driven removal near the coast (0–60 km) (Figures 2c and 3d) to a mix of supply and removal in the transition (60–200 km) and offshore regions (>200 km) (Figures 2d and 3d).

In summary, the 1 km simulation highlights a regional and temporally dynamical role for eddies in the California Current. In wintertime and in the offshore region, the picture is similar to what occurs in the oligotrophic, permanently stratified ocean, where eddy-induced vertical nutrient fluxes enhance biological activity (Mahadevan, 2016; McGillicuddy Jr, 2016). In the coastal region, following upwelling, eddies remove nutrients from the surface, counterbalancing and even offsetting wind-driven upwelling, and ultimately limiting primary production (Gruber et al., 2011).

The effect of eddies stems from a combination of transports that occur at scales ranging from mesoscale to submesoscale (Capet, Klein, et al., 2008). Because submesoscale dynamics intensifies cyclonic circulation, surface convergence, and downwelling, in particular near the coastal upwelling front, it is likely an important element behind eddy quenching. Similarly, higher variability and intensity of vertical velocities at submesoscale (Figure 4) likely enhance vertical mixing and upward nutrient fluxes in the offshore oligotrophic region. In the following section, we focus on the submesoscale component of this vertical transport.

4. Submesoscale Intensification of Nutrients Transport

We investigate the role of submesoscale currents for NO_3^- fluxes by comparing the 1 and 4 km simulations. As discussed in section 2.2, the 1 km solution displays the typical hallmarks of submesoscale dynamics. Thus, we attribute the difference between the 1 and 4 km solutions to this submesoscale circulation component. We focus on the coastal (0–50 km) and offshore (>250 km) regions, where two different regimes (eddy removal and eddy supply of nutrients, respectively) have been discussed in the previous section.

The variability of the vertical eddy flux of NO_3^- ($\overline{w'\text{NO}_3^{-'}}$) at 50 m depth for the coastal domain is shown in Figure 4a. Maximum eddy fluxes are greatly enhanced at 1 km resolution, by approximately 1 order of magnitude. The time series also shows a strong compensation between upward and downward fluxes, such that climatological averages (e.g., Figures 2c, 2d, 3c, and 3d) represent a small residual of large opposing terms. In the 1 km simulation, “bursts” of intense vertical nutrient supply occur over time scales of few days or less, generally associated with intensification of fronts and filaments. These intense submesoscale episodes cluster together in time, occurring more frequently during upwelling, in particular near the coast.

The much larger intensity of vertical eddy nutrient fluxes at 1 km is encapsulated by the probability density function (PDF) of $w'\text{NO}_3^{-'}$, shown in Figure 4b and the statistics summarized in supporting information Table S2. Consistent with the submesoscale intensification, the variance of $\overline{w'\text{NO}_3^{-'}}$ increases by approximately 1 order of magnitude going from the 4 to the 1 km simulation. In the coastal region, this increase is stronger during upwelling, when baroclinic instabilities are more common and intense.

A different picture characterizes the offshore region, where the variability of $\overline{w'\text{NO}_3^{-'}}$ in the 1 km simulation, as compared to the 4 km simulation, is much larger in winter. This reflects a greatly increased submesoscale activity at the time of the year characterized by deeper mixed layers. Similarly to the variance, the kurtosis, or “tailedness” of the $w'\text{NO}_3^{-'}$ PDF is also enhanced at 1 km (supporting information Table S2), reflecting the increased intermittency and frequency of the transport extremes at submesoscale fronts. The negative skewness of the PDF also confirms the dominance of downwelling over upwelling extremes.

The climatological cycles of the eddy fluxes of NO_3^- in the 4 and 1 km solutions are shown in Figures 2e and 2f, together with their difference, which we take as a measure of the impact of the resolved submesoscale circulation. In the California Current, the role of the submesoscale circulation roughly mirrors the overall role of eddy fluxes, with some notable differences.

Near the coast, submesoscale currents drive an intensification of eddy quenching; that is, they enhance transport of nutrients away from the euphotic zone (Figure 2e). This subduction is particularly intense at the onset of upwelling and lasts throughout the spring and early summer. However, it becomes negligible or even reverses sign in the fall. Notably, during winter, the 4 km simulation suggests a slightly positive eddy flux of nutrients at mesoscale; this flux becomes negligible or slightly negative in the 1 km simulation. Thus, in this region and time of the year, submesoscale currents can reverse the sign of the eddy nutrient fluxes. Offshore, submesoscale currents increase the eddy supply of nutrients to the surface. This intensification is stronger in fall and winter and becomes weaker during late upwelling and summer.

Together with significant seasonal variations, eddy nutrient fluxes are influenced by interannual variability, as illustrated by the intense 1997–1998 El Niño, sandwiched between normal years (Figure 4a). As part of the 1998 El Niño, vertical eddy fluxes strongly decline in the coastal region during the winter and upwelling seasons and nearly collapse in the offshore region during spring. During these periods, submesoscale activity is not greatly impacted. The main reason for the strong reduction in vertical nutrient fluxes is the deepening of the nutricline during El Niño, so that the bulk of nutrients are found a few tens of meters below the mixed layer, where submesoscale activity is weaker.

5. Submesoscale Modulation of Ecosystem Processes

Consistent with previous studies (Lévy et al., 2009; Mahadevan et al., 2012), the spatial distribution of surface phytoplankton is affected by variability at both mesoscale and submesoscale. High concentrations of chlorophyll (Figure 5a and supporting information Figure S7c) are associated with cold filaments originating from recently upwelled waters. These features show a rich submesoscale structure in the 1 km model, with multiple fronts at scales of few kilometers, surrounded by patches of high and low chlorophyll within

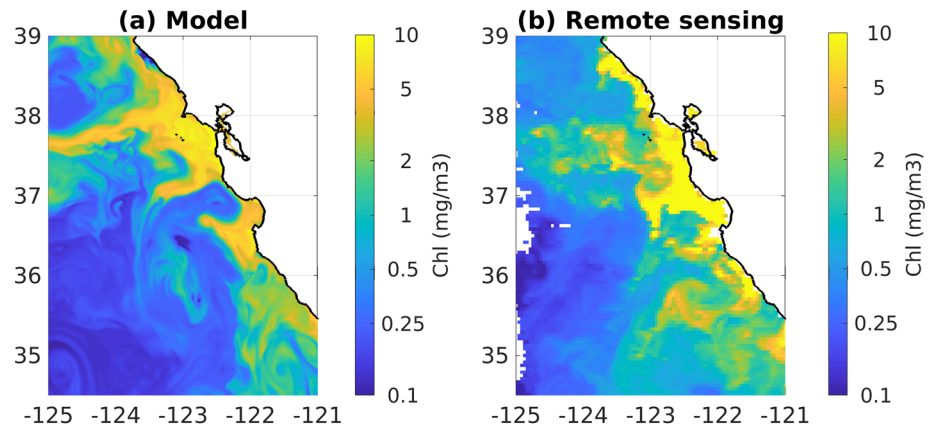


Figure 5. Modeled and observed submesoscale patterns in surface chlorophyll. (a) Daily mean average surface chlorophyll concentration (mg Chl m^{-3}) from the 1 km model simulation, for the day of 12 October 2005. (b) Remote sensing image of surface chlorophyll from the GlobColour Project for the day of 16 October 2016, at 4 km resolution (date chosen based on lack of cloud cover). Note the similar submesoscale features in the model and observations.

submesoscale eddies, in remarkable agreement with remote sensing observations (Figure 5b). In the following, we quantify the biological effects of this submesoscale heterogeneity on productivity and organic matter cycles.

The climatological seasonal cycle of primary production, as a function of distance from the coast, is shown in Figure 6a, revealing the coastal intensification at the beginning of the upwelling period, and the offshore maximum in winter. Primary production is enhanced at submesoscale over most of the domain, by up to 20% (Figure 6b). The offshore intensification is consistent with the increased vertical flux of nutrients in oligotrophic waters and peaks in summer. The absolute maximum increase in primary production is observed in the intermediate band between 40 and 200 km following upwelling (see also Figures 7a and 7c for the annual mean response).

We speculate that this enhancement is driven by increased nutrient subduction and transport from the coastal region and resupply by vertical submesoscale fluxes. Only near the coast in late summer and fall does primary production slightly decrease at submesoscale, presumably due to more intense subduction by eddies. The fraction of primary production fueled by newly upwelled NO_3^- , that is, the f ratio, is largest in the nearshore band during upwelling (around 0.4 on average, and up to 0.6) and decreases to low background values (less than 0.1) in the oligotrophic region offshore (Figure 7b and supporting information Figure S8). As expected, submesoscale circulation decreases new production nearshore while dramatically increasing it offshore.

Phytoplankton biomass is characterized by a seasonal cycle that closely follows that of primary production (Figure 6c), with a dominance of diatoms as far as 300 km offshore (Figure 7b and supporting information Figure S9). Zooplankton follow a somewhat different cycle (Figure 6e), with enhanced biomass offshore, in particular in late winter, and a reduction near the coast that is significant during upwelling. We attribute this coastal reduction to offshore Ekman transport and subduction, combined with the inherently slower zooplankton growth rate, which limit biomass accumulation near the coast.

The submesoscale modulation of phytoplankton and zooplankton biomass (Figures 6d and 6f) is similar to that of primary production (Figure 6b). Submesoscale circulation drives an increase in biomass offshore throughout the year and a decrease from the coast to the intermediate region during the late upwelling, summer, and fall. These changes are stronger for phytoplankton, with an increase of more than 30% offshore during upwelling, as compared to about 10% for zooplankton. The biomass reduction reflects the combined effects of declining nutrient supply and primary production at submesoscale and increasing subduction of planktonic cells by eddies. These changes are accompanied by similar changes in the abundance of diatoms, which decrease in the coastal and intermediate bands and increase offshore (Figure 7d).

In the model, the fraction of primary production that enters the food web (i.e., the z ratio Stock & Dunne, 2010) reaches up to 40% offshore, where small cells and the microbial loop dominate (Figure 7b and

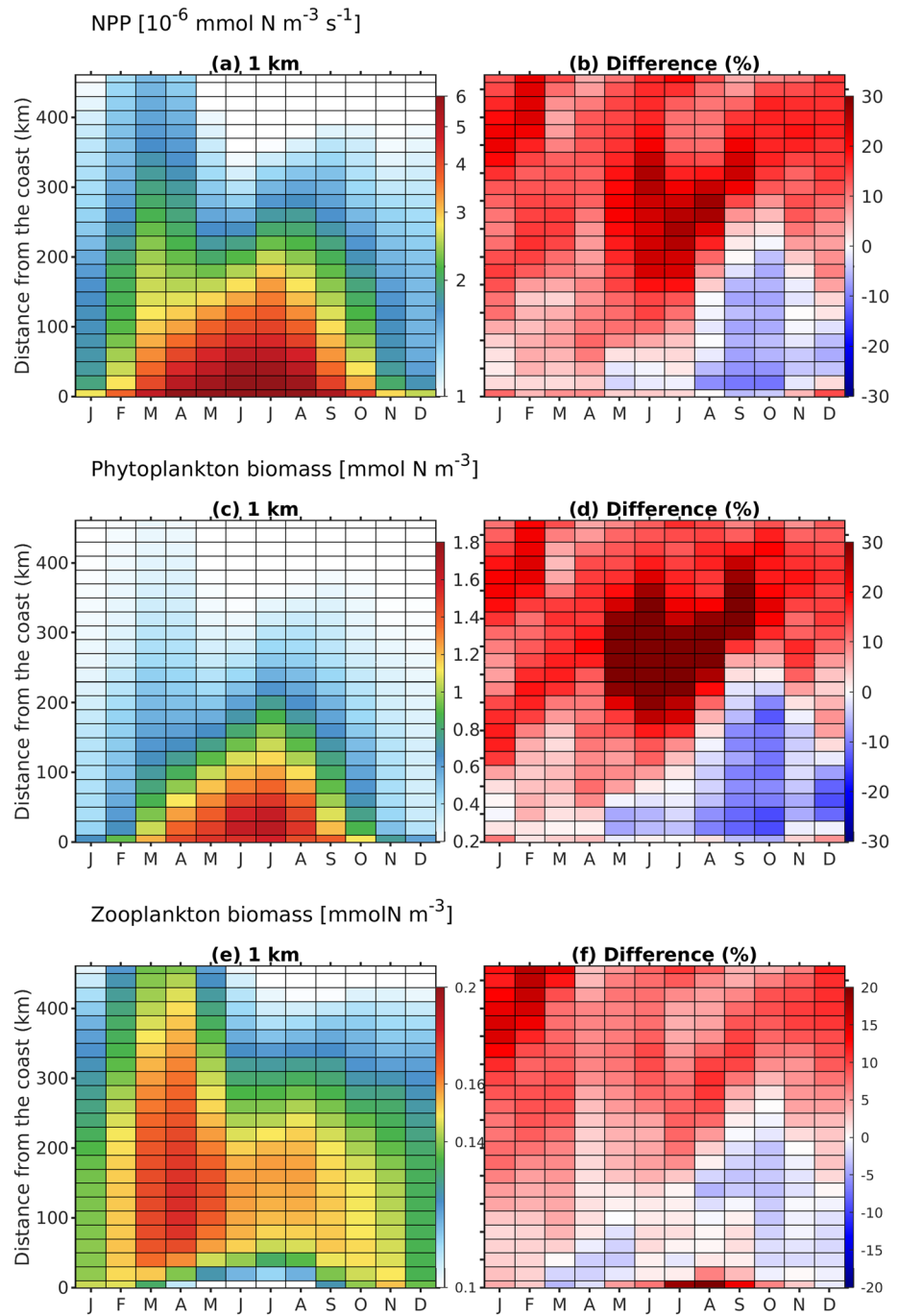


Figure 6. Climatological Hovmöller diagrams of (a, b) total primary production; (c, d) phytoplankton biomass; and (e, f) zooplankton biomass, averaged alongshore for the analysis region shown in Figure 1. The x axis shows climatological month, and the y axis distance from the coast. The panels on the left (a, c, e) show values from the 1 km solution, the right panels (b, d, f) the relative difference (%) between the 1 and 4 km solutions. Values are 0–50 m depth averages.

supporting information Figure S9). This proportion decreases to smaller values (<20%) nearshore, in particular during upwelling, due to a combination of high primary production, low zooplankton biomass, and large organic matter export. We observe a slight reduction (<5%) of the z ratio at submesoscale (Figure 7d and supporting information Figure S10), in particular in the intermediate region following upwelling.

Organic matter fixed by photosynthesis accumulates as living organisms and dissolved detritus and is exported from the surface by sinking particles and physical transport. The sinking particle export (Figure 7a

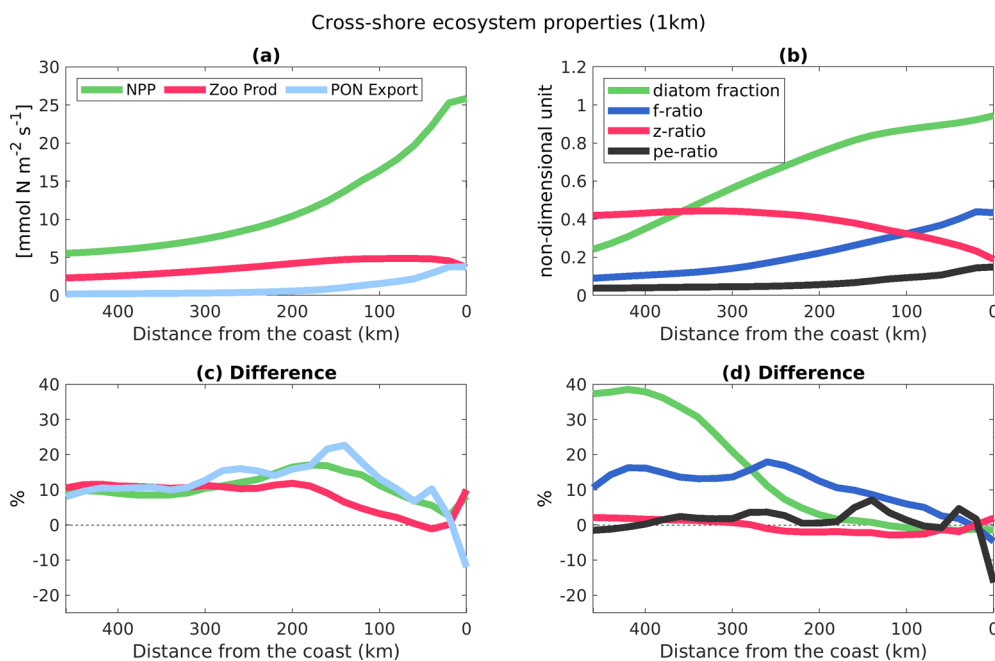


Figure 7. The 10 year mean of biogeochemical properties from the 1 km model solution, as a function of the distance from the coast. (a) Annual mean primary production, zooplankton production, and particulate organic matter export ($\text{mmol N m}^{-2} \text{s}^{-1}$). (b) Annual mean diatom fraction, *f* ratio, *z* ratio, and *pe* ratio. (c) Relative difference (%) between the 1 and 4 km solutions ($100 \times [1 \text{ km} - 4 \text{ km}]/4 \text{ km}$ for the quantities shown in (a), and (d) relative difference between the 1 and 4 km solutions ($100 \times [1 \text{ km} - 4 \text{ km}]/4 \text{ km}$ for the quantities shown in (b).

and supporting information Figure S11) follows the patterns of primary production and peaks near the coast during upwelling. Compared to primary production, export declines faster with the distance from the coast, as indicated by the particle export ratio (*pe* ratio Dunne et al., 2005), the fraction of organic matter that is exported by sinking particles (Figure 7b and supporting information Figure S12). Values up to 20%, typical of productive regions, are observed during upwelling in the 50–100 km band and decline offshore to less than 5%, typical of the oligotrophic ocean.

The submesoscale modulation of particle export consists of an overall increase by 10–20% up to 250km, and 10% further offshore, with the exception of the very nearshore band, where a decline is observed (Figure 7c), driving also a similar decline in the *pe* ratio (Figure 7d). In the intermediate and the offshore regions, besides a small increase in the *pe* ratio by less than 10% between 100 and 200km (Figure 7d), primary production and particle export increase at a similar pace, leaving the *pe* ratio nearly unchanged.

Physical transport of nonsinking organic matter varies seasonally with the cycle of primary production (Figure 8), peaking during the upwelling season and reaching a minimum during the fall. We identify an important submesoscale intensification of this physical transport, reaching up to 30% during the upwelling season. We attribute this intensification to submesoscale eddies, which enhance subduction of dissolved organic matter and living cells away from the euphotic zone.

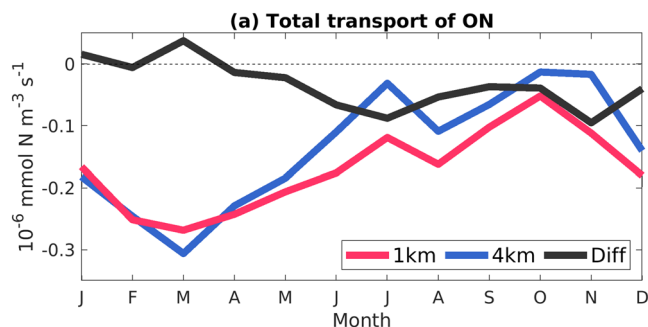


Figure 8. The 10 year climatological mean of organic nitrogen (ON) transport ($\text{mmol N m}^{-3} \text{s}^{-1}$) from the budget analysis domain (see Figure 1, here shown for the depth range between 0 and 50 m). The blue line shows the 4 km solution, the red line the 1 km solution, and the black line the difference between the 1 and 4 km solutions. Negative values show export from the domain. Total transport includes both vertical and horizontal contributions.

6. Summary and Conclusions

Previous studies have highlighted the seasonal cycle and geographical variability of submesoscale currents in the California Current System (Capet, Campos, et al., 2008; Capet, Klein, et al., 2008; Capet, McWilliams, et al., 2008; Molemaker et al., 2015; McWilliams, 2016). Other studies have shown the impact of submesoscale circulation on primary production using idealized simulations of the open ocean

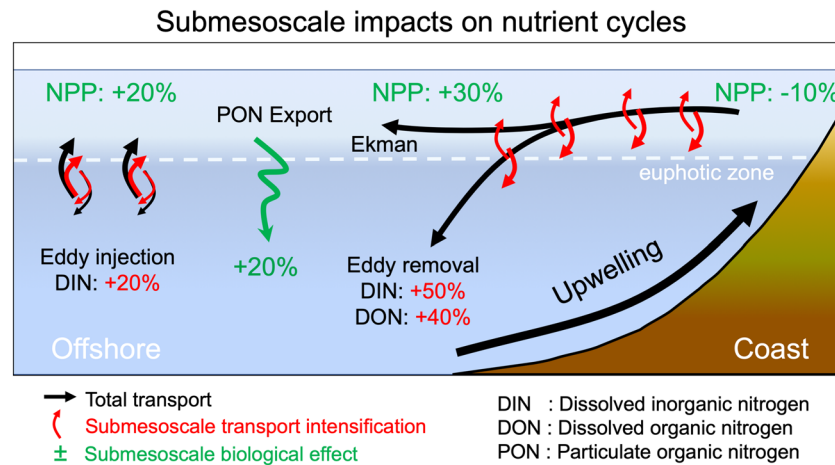


Figure 9. Schematic of the role of submesoscale circulation for nutrient and organic matter dynamics in the California Current System. Numbers show the difference between the 1 and 4 km model simulations and represent maximum monthly changes observed over the course of a climatological year.

(Lévy et al., 2012; Mahadevan et al., 2012; Mahadevan, 2016). Our study is the first to quantify the impact of submesoscale circulation on nutrient and organic matter cycles in a realistic representation of this eastern boundary upwelling system.

In a general way, we find that (1) in the coastal region, submesoscale eddies increase nutrient and organic matter subduction, further counteracting wind-driven upwelling and reducing productivity (i.e., intensifying “eddy quenching”); (2) in the offshore oligotrophic region, submesoscale eddies enhance the delivery of nutrients to the surface, fueling an increase in new production; (3) these submesoscale effects are modulated by the seasonal cycle and are more intense in the coastal band during upwelling and in the offshore band in winter. Analogous processes are likely to occur in other regions characterized by similar dynamics, that is, other eastern boundary upwelling systems. However, the magnitude and relative importance of submesoscale processes would depend on the specific conditions of the region considered.

The biogeochemical impacts of submesoscale currents on nutrient cycles in the California Current are summarized in Figure 9. At the root of these impacts is the covariation between vertical velocities and nutrient anomalies, which results in vigorous vertical eddy fluxes that are intensified at submesoscale. In the coastal region, submesoscale processes strengthen convergence and downwelling in cyclonic patches of cold, nutrient-rich waters. The effect is an enhancement of nutrient subduction, in particular, following upwelling. In the offshore region, deepening of the nutricline reverses the covariation between surface nutrients and vertical velocities to typical open-ocean conditions, such that transient eddies supply nutrient-rich waters to the surface, while subducting nutrient-depleted waters. The result is a net upward flux of nutrients which is enhanced at submesoscale, in particular during periods of deeper mixed layers, that is, wintertime.

Changes in turbulent fluxes at submesoscale modulate primary production, plankton dynamics, and export (Figure 9). First, submesoscale currents increase new production and plankton biomass in the oligotrophic waters offshore, favoring large phytoplankton. Second, they drive a decline of new production and biomass in the coastal and intermediate regions, reducing the abundance of large phytoplankton. These effects reverberate through the food web, resulting in similar, albeit weaker changes in zooplankton abundance and productivity. Finally, submesoscale currents drive an overall strengthening of organic matter export, by increasing both sinking particle fluxes and organic matter subduction nearly everywhere.

Our results confirm that submesoscale currents play a major role for ocean biogeochemistry (Lévy et al., 2018; Mahadevan, 2016) and that their impact on the surface ecosystem can be dramatically different depending on the region and time of the year. While these conclusions appear robust and general, there are some caveats to our study. Our highest-resolution configuration is able to capture the physical transition between mesoscale and submesoscale but likely underestimates the magnitude of submesoscale currents and the associated eddy fluxes. We speculate that increasing model resolution to scales of hundreds of meters

or smaller would produce changes in the same direction discussed in this study and likely greater magnitude. For example, preliminary results with a similar configuration, run with a horizontal grid scale of $dx = 300$ m, suggest a further increase of the range of vertical eddy fluxes (the quantity shown in Figure 4a) by up to 3 times.

We also based our analysis on daily averages of model output. Thus, we have not directly investigated variability associated with the diurnal cycle and aspects of frontogenesis and other processes that occur at time scales faster than a day. Analysis of output saved at 4 hr frequency likewise indicates an increase of the range of vertical eddy fluxes of nutrients by about 50%. Limitations in our analysis reflect choices dictated by computational and storage constraints, which will be addressed in future studies. We also adopted a widely used but simple ecological model, with a minimal representation of phytoplankton diversity, a single zooplankton group, and implicit representation of sinking particles.

It is likely that the increase in environmental heterogeneity at submesoscale is an important factor in shaping the size structure, diversity, and interaction of phytoplankton, zooplankton, and their predators (Lévy et al., 2018; Martin, 2003; Woodson & Litvin, 2015). Furthermore, vigorous transport along submesoscale fronts would influence the dynamics and magnitude of sinking particle export (Stukel et al., 2017). Capturing the full range of processes and ecological implications of submesoscale heterogeneity and transport will likely require more sophisticated models of the ocean food web, coupled to physical models with a resolution of the order of hundreds of meters or less.

Data Availability Statement

The model code and the scripts and data used to create the figures are available online (following the DOI:10.5281/zenodo.4033286). Raw model output can be obtained from the Authors upon request.

Acknowledgments

This research was supported by NSF grant OCE-1419323, NOAA grants NA15NOS4780186 and NA18NOS4780174, and California Ocean Protection Council grant C0100400. Computational resources were provided by the Extreme Science and Engineering Discovery Environment (XSEDE) through allocation TG-OCE170017.

References

- Boccaletti, G., Ferrari, R., Adcroft, A., Ferreira, D., & Marshall, J. (2005). The vertical structure of ocean heat transport. *Geophysical Research Letters*, *32*, L10603. <https://doi.org/10.1029/2005GL022474>
- Capet, X., Campos, E. J., & Paiva, A. M. (2008). Submesoscale activity over the Argentinian shelf. *Geophysical Research Letters*, *35*, L15605. <https://doi.org/10.1029/2008GL034736>
- Capet, X., Klein, P., Hua, B. L., Lapeyre, G., & McWilliams, J. C. (2008). Surface kinetic energy transfer in surface quasi-geostrophic flows. *Journal of Fluid Mechanics*, *604*, 165–174.
- Capet, X., McWilliams, J. C., Molemaker, M. J., & Shchepetkin, A. F. (2008). Mesoscale to submesoscale transition in the California Current System. Part I: Flow structure, eddy flux, and observational tests. *Journal of Physical Oceanography*, *38*(1), 29–43.
- Chavez, F. P., & Messié, M. (2009). A comparison of eastern boundary upwelling ecosystems. *Progress in Oceanography*, *53*(1–4), 80–96.
- Cochrane, K., De Young, C., Soto, D., & Bahri, T. (2009). Climate change implications for fisheries and aquaculture. *FAO Fisheries and Aquaculture Technical Paper*, *530*, 212.
- Deutsch, C. A., Frenzel, H., McWilliams, J. C., Renault, L., Kessouri, F., Howard, E. M., et al. (2020). Biogeochemical variability in the California Current System. *bioRxiv*, *2*(10), 942565. <https://doi.org/10.1101/2020.02.10.942565>
- Dunne, J. P., Armstrong, R. A., Gnanadesikan, A., & Sarmiento, J. L. (2005). Empirical and mechanistic models for the particle export ratio. *Global Biogeochemical Cycles*, *19*(4), GB4026.
- Gruber, N., Lachkar, Z., Frenzel, H., Marchesiello, P., Münnich, M., McWilliams, J. C., et al. (2011). Eddy-induced reduction of biological production in eastern boundary upwelling systems. *Nature geoscience*, *4*(11), 787.
- Huyer, A. (1983). Coastal upwelling in the California Current system. *Progress in Oceanography*, *12*(3), 259–284.
- Lathuilière, C., Echevin, V., Lévy, M., & Madec, G. (2010). On the role of the mesoscale circulation on an idealized coastal upwelling ecosystem. *Journal of Geophysical Research*, *115*, C09018. <https://doi.org/10.1029/2009JC005827>
- Lévy, M., Ferrari, R., Franks, P. eterJ. S., Martin, A. P., & Rivière, P. (2012). Bringing physics to life at the submesoscale. *Geophysical Research Letters*, *39*, L14602. <https://doi.org/10.1029/2012GL052756>
- Lévy, M., Franks, P. eterJ. S., & Smith, K. S. (2018). The role of submesoscale currents in structuring marine ecosystems. *Nature communications*, *9*(1), 4758.
- Lévy, M., Klein, P., & Ben Jelloul, M. (2009). New production stimulated by high-frequency winds in a turbulent mesoscale eddy field. *Geophysical Research Letters*, *36*, L16603. <https://doi.org/10.1029/2009GL039490>
- Lévy, M., Klein, P., & Treguier, A.-M. (2001). Impact of sub-mesoscale physics on production and subduction of phytoplankton in an oligotrophic regime. *Journal of Marine Research*, *59*(4), 535–565.
- Lévy, M., & Martin, A. P. (2013). The influence of mesoscale and submesoscale heterogeneity on ocean biogeochemical reactions. *Global Biogeochemical Cycles*, *27*(4), 1139–1150.
- Lovecchio, E., Gruber, N., & Münnich, M. (2018). Mesoscale contribution to the long-range offshore transport of organic carbon from the Canary Upwelling System to the open North Atlantic. *Biogeosciences*, *15*(16), 5061–5091.
- Mahadevan, A. (2016). The impact of submesoscale physics on primary productivity of plankton. *Annual Review of Marine Science*, *8*, 161–184.
- Mahadevan, A., D'Asaro, E., Lee, C., & Perry, M. J. (2012). Eddy-driven stratification initiates North Atlantic spring phytoplankton blooms. *Science*, *337*(6090), 54–58.
- Marchesiello, P., McWilliams, J. C., & Shchepetkin, A. (2003). Equilibrium structure and dynamics of the California Current System. *Journal of Physical Oceanography*, *33*(4), 753–783.

- Martin, A. P. (2003). Phytoplankton patchiness: The role of lateral stirring and mixing. *Progress in Oceanography*, *57*(2), 125–174.
- Martin, A. P., Lévy, M., Gennip, S., Pardo, S., Srokosz, M., Allen, J., et al. (2015). An observational assessment of the influence of mesoscale and submesoscale heterogeneity on ocean biogeochemical reactions. *Global Biogeochemical Cycles*, *29*(9), 1421–1438.
- McGillicuddy Jr, D. J. (2016). Mechanisms of physical-biological-biogeochemical interaction at the oceanic mesoscale. *Annual Reviews of Marine Science*, *8*, 125–159.
- McWilliams, J. C. (2007). Irreducible imprecision in atmospheric and oceanic simulations. *Proceedings of the National Academy of Sciences*, *104*(21), 8709–8713.
- McWilliams, J. C. (2016). Submesoscale currents in the ocean. *Proceedings of the Royal Society A: Mathematical, Physical and Engineering Sciences*, *472*(2189), 20160117.
- Molemaker, M. J., McWilliams, J. C., & Dewar, W. K. (2015). Submesoscale instability and generation of mesoscale anticyclones near a separation of the California Undercurrent. *Journal of Physical Oceanography*, *45*(3), 613–629.
- Moore, J. K., Doney, S. C., & Lindsay, K. (2004). Upper ocean ecosystem dynamics and iron cycling in a global three-dimensional model. *Global Biogeochemical Cycles*, *18*(4), GB4028. <https://doi.org/10.1029/2004GB002220>
- Nagai, T., Gruber, N., Frenzel, H., Lachkar, Z., McWilliams, J. C., & Plattner, G.-K. (2015). Dominant role of eddies and filaments in the offshore transport of carbon and nutrients in the California Current System. *Journal of Geophysical Research: Oceans*, *120*, 5318–5341. <https://doi.org/10.1002/2015JC010889>
- Omand, M. M., D'Asaro, E. A., Lee, C. M., Perry, M. J., Briggs, N., Cetinić, I., & Mahadevan, A. (2015). Eddy-driven subduction exports particulate organic carbon from the spring bloom. *Science*, *348*(6231), 222–225.
- Renault, L., Deutsch, C., McWilliams, J. C., Frenzel, H., Liang, J.-H., & Colas, F. (2016). Partial decoupling of primary productivity from upwelling in the California Current System. *Nature Geoscience*, *9*(7), 505.
- Renault, L., Hall, A., & McWilliams, J. C. (2016). Orographic shaping of U.S. West Coast wind profiles during the upwelling season. *Climate Dynamics*, *46*, 273–289.
- Renault, L., Masson, S., Arsouze, T., Madec, G., & McWilliams, J. C. (2020). Recipes for how to force oceanic model dynamics. *Journal of Advances in Modeling Earth Systems*, *12*, e2019MS001715.
- Renault, L., McWilliams, J. C., & Gula, J. (2018). Dampening of submesoscale currents by air-sea stress coupling in the Californian upwelling system. *Scientific reports*, *8*(1), 13388.
- Renault, L., McWilliams, J. C., Jousse, A., Deutsch, C., Frenzel, H., Kessouri, F., & Chen, R. (2020). The physical structure and behavior of the California Current System. *bioRxiv*, *02*(10), 942730. <https://doi.org/10.1101/2020.02.10.942730>
- Renault, L., Molemaker, M. J., McWilliams, J. C., Shchepetkin, A. F., Lemarié, F., Chelton, D., et al. (2016). Modulation of wind work by oceanic current interaction with the atmosphere. *Journal of Physical Oceanography*, *46*(6), 1685–1704.
- Shchepetkin, A. F. (2015). An adaptive, courant-number-dependent implicit scheme for vertical advection in oceanic modeling. *Ocean Modelling*, *91*, 38–69.
- Shchepetkin, A. F., & McWilliams, J. C. (2005). The Regional Oceanic Modeling System (ROMS): A split-explicit, free-surface, topography-following-coordinate oceanic model. *Ocean modelling*, *9*(4), 347–404.
- Shchepetkin, A. F., & McWilliams, J. C. (2009). Correction and commentary for “Ocean forecasting in terrain-following coordinates: Formulation and skill assessment of the regional ocean modeling system” by Haidvogel et al., *J. Comp. Phys.* *227*, pp. 3595–3624. *Journal of Computational Physics*, *228*(24), 8985–9000.
- Skamarock, W. C., & Klemp, J. B. (2008). A time-split nonhydrostatic atmospheric model for weather research and forecasting applications. *Journal of Computational Physics*, *227*(7), 3465–3485.
- Srinivasan, K., McWilliams, J. C., Renault, L., Hristova, H. G., Molemaker, J., & Kessler, W. S. (2017). Topographic and mixed layer submesoscale currents in the near-surface southwestern tropical Pacific. *Journal of Physical Oceanography*, *47*(6), 1221–1242. <https://doi.org/10.1175/JPO-D-16-0216.1>
- Stock, C., & Dunne, J. (2010). Controls on the ratio of mesozooplankton production to primary production in marine ecosystems. *Deep Sea Research Part I: Oceanographic Research Papers*, *57*(1), 95–112.
- Stukel, M. R., Aluwihare, L. I., Barbeau, K. A., Chekalyuk, A. M., Goericke, R., Miller, A. J., et al. (2017). Mesoscale ocean fronts enhance carbon export due to gravitational sinking and subduction. *Proceedings of the National Academy of Sciences*, *114*(6), 1252–1257.
- Thomas, H., Schiettecatte, L.-S., Suykens, K. O. N. E., Kone, Y. J. M., Shadwick, E. H., Prowe, A. E. F., et al. (2008). Enhanced ocean carbon storage from anaerobic alkalinity generation in coastal sediments. *Biogeosciences*, *6*, 267–274.
- Woodson, C. B., & Litvin, S. Y. (2015). Ocean fronts drive marine fishery production and biogeochemical cycling. *Proceedings of the National Academy of Sciences*, *112*(6), 1710–1715.